

## TUNABLE Au/Ga<sub>2</sub>S<sub>3</sub>/Yb VARACTOR DIODES DESIGNED FOR HIGH FREQUENCY APPLICATIONS

S. E. AL GARNI<sup>a\*</sup>, A. F. QASRAWI<sup>b</sup>

<sup>a</sup>*Physics Department, Faculty of Science- Al Faisaliah, King Abdulaziz University, Jeddah- Saudi Arabia*

<sup>b</sup>*Departments of Physics at AAUP, Jenin and Group of physics, Faculty of Engineering, Atilim University, 06836 Ankara, Turkey*

In this work, the design and characterization of Au/Ga<sub>2</sub>S<sub>3</sub>/Yb Schottky barrier is investigated by means of transmittance electron microscopy (TEM), scanning electron microscopy (SEM), energy dispersive X-ray spectroscopy (EDXS), capacitance spectroscopy, capacitance (C)-voltage (V) characteristics and impedance spectroscopy techniques. The design of the energy band diagram of the amorphous Au/Ga<sub>2</sub>S<sub>3</sub> interface revealed a theoretical energy barrier height ( $q\phi_b$ ) and built in voltage ( $qV_{bi}$ ) of 2.04 and 1.88 eV, respectively. Experimentally, the  $qV_{bi}$  was observed to be sensitive to the applied signal frequency. In addition, the capacitance spectra which were studied in the range of 10-1800 MHz, revealed resonance and antiresonance biasing dependent signal oscillations associated with negative capacitance values. On the other hand, impedance spectroscopy analysis revealed band pass/reject filtering properties in all the studied frequency range. The device exhibited a return loss, voltage standing wave ratio and power efficiency of 16.7 dB, 1.3 and 98.3% at 1400 MHz, respectively.

(Received June 28, 2017; Accepted September 8, 2017)

*Keyword:* Thin films; Vapor deposition; Electron microscopy; X-ray diffraction; Dielectrics; Electrical properties

### 1. Introduction

Ga<sub>2</sub>S<sub>3</sub> is a compound that recently reported to be have smart features for visible light, microwave and infrared technological applications [1-5]. This compound is found to exhibit a maximal transparency in the range of 0.48-22.5  $\mu\text{m}$ . In that range of spectral response, owing its anisotropic properties, the Ga<sub>2</sub>S<sub>3</sub> is attractive for use in nonlinear optical applications [1]. In addition, the three dimensional Ga<sub>2</sub>S<sub>3</sub> is suggested as a competitor to the layered GaSe and its solid solutions which possess outstanding optical properties. Both compounds are candidates for THz applications [2, 3]. Moreover, the photoluminescence spectral studies have shown that there exist a defect (excited Ga vacancies) related red (1.62 eV) and green (2.24 eV) emission lines in the Ga<sub>2</sub>S<sub>3</sub> films [4]. The *p*-Ga<sub>2</sub>S<sub>3</sub>/*n*-GaAs heterojunction displayed a large on/off current ratio under a blue laser (405 nm, 3.0 mW) illumination nominating it as high-power laser radiation sensor [4]. On the other hand, earlier studies of the temperature dependent Electrical and photoelectrical properties of the *p*-Si/ *n*-(Ga<sub>2</sub>Se<sub>3</sub>-Ga<sub>2</sub>S<sub>3</sub>) thin films heterojunctions have shown that, the photovoltaic device reveal an open-circuit voltage of 0.70 V, a short-circuit current density of 9.42 mA cm<sup>-2</sup> and a power conversion efficiency of 5.20% [5].

In our previous work, we have investigated the dielectric dispersion properties of the Ga<sub>2</sub>S<sub>3</sub> thin films which are deposited onto glass substrates [3]. The modeling of the dielectric spectra for these films in the frequency range of 270–1,000 THz, using the modified Drude-Lorentz model for electron-plasmon interactions revealed electron bound plasma frequencies in the range of  $\sim 0.76\text{--}0.94$  (GHz). The corresponding drift mobility of electrons in the terahertz oscillating incident electric field was found to be 7.91 (cm<sup>2</sup>/Vs). The values are motivating for employing the Ga<sub>2</sub>S<sub>3</sub> thin films as tunable capacitor capable of resonating electrical signals at high

---

\* Correspond author: seef73@gmail.com

frequencies. Thus, here in this work, we will discuss the design and characterization of the Au/Ga<sub>2</sub>S<sub>3</sub>/Yb device as a promising circuit element. Particularly, we will explore the capacitance spectra in the frequency range of 10-1800 MHz. In addition, the voltage biasing effect on the diode performance will be studied and analyzed to determine the device operational parameters. The frequency dependent voltage biasing of the Au/Ga<sub>2</sub>S<sub>3</sub>/Yb capacitors will be studied and analyzed to determine the wave trapping features of the device.

## 2. Experimental details

Both of the Au, Yb and the Ga<sub>2</sub>S<sub>3</sub> thin films were deposited using the vacuum evaporation technique with the help of VCM600 thermal evaporator at a vacuum pressure of 10<sup>-5</sup> mbar. Each of the films was of 1.0 μm thicknesses. The obtained Au films were used as substrates to evaporate the Ga<sub>2</sub>S<sub>3</sub>. The X-ray diffraction patterns for the glass/ Ga<sub>2</sub>S<sub>3</sub> and Au/Ga<sub>2</sub>S<sub>3</sub> interface were recorded using Rigako Ultima IV X-ray diffraction unit. The surface morphology and composition was studied using scanning electron microscopy with a JOEL JSM 7600F instrument that has an energy dispersion X-ray spectrometer (EDXS). The transmittance electron microscopy (JEOL JEM-1230) operating at 120 kV attached to a CCD camera was employed to reveals more deep analysis of the Ga<sub>2</sub>S<sub>3</sub> film properties. On the other hand, the electrical characterizations were actualized with the help of an automated Keithley system that is equipped with a pico-ammeter and voltage source. The impedance spectra were recorded using Agilent 4291B 10-1800 MHz impedance analyzer.

## 3. Results and discussion

One of the best recorded scanning electron microscopic images for the Ga<sub>2</sub>S<sub>3</sub> films deposited onto Au substrates is shown in Fig. 1 (a). The image which is recorded at low field of 5 kV for a 60000 magnification ratio reveal no well resolved structure. Some rarely observed bright grains of size of ~ 50 nm appeared in then SEM image. The SEM image did not display any clear distribution of the grains. Even though, when the energy dispersive X-ray spectroscopy analysis was used to determine the composition of the grown films, the EDXS signals displayed atomic content of 40.7% Ga and 59.3% S atomic contents assuring the stoichiometric growth of the Ga<sub>2</sub>S<sub>3</sub> films. To reveal more detailed analysis, the transmittance electron microscopy was used to observe the film structure. The resulting images are displayed in Fig. 1 (b) and (c). While the image of (b) showing the two species which are used for analysis, that of (c) illustrate uniform and weak agglomerated Ga<sub>2</sub>S<sub>3</sub> nanospheres with diameter of 7-8 nm. The nanospheres are randomly and intensively distributed. No specific structure was resolved from the TEM images indicating the amorphous nature of structure. On the other hand, the X-ray diffraction data which are shown in Fig. 1 (d) compares, the films which are deposited onto glass substrates with those deposited onto face centered cubic (*fcc*) Au substrate of plane orientation in the (111) direction. Whereas no intensive peaks are observed in the X-ray diffraction patterns of the Ga<sub>2</sub>S<sub>3</sub> films deposited onto glass substrates, the X-ray diffraction patterns for the films deposited onto Au substrate contained strong peaks of Au film [6] and one broaden peak of Ga<sub>2</sub>S<sub>3</sub>.

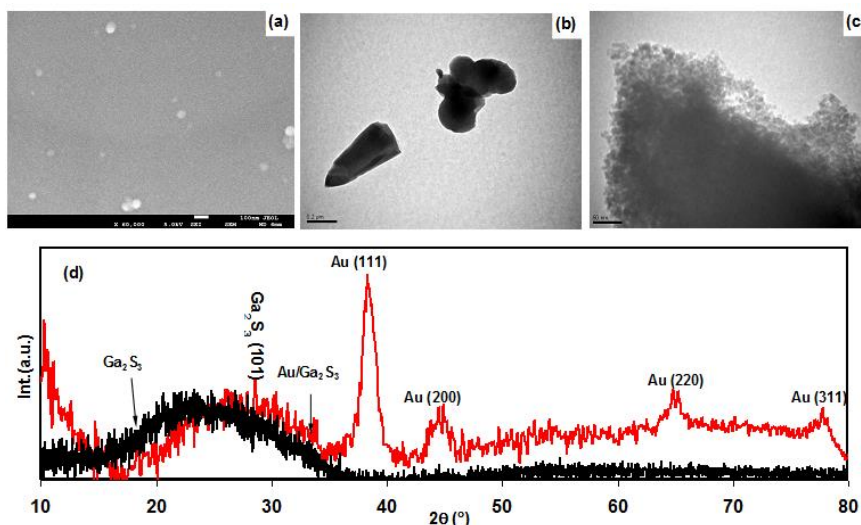


Fig. 1 (a) The SEM images for a magnification of 60,000 , (b) The TEM image for a 50,000 and (c) for 200,000 times, and (d) the X-ray diffraction patterns for  $\text{Ga}_2\text{S}_3$  films.

The  $\text{Ga}_2\text{S}_3$  compound is known to exhibit monoclinic, hexagonal and cubic crystal phases that appear at the same angles in the X-ray diffraction curves [4, 7]. Such a property appears as a result of the existence of the small distortions in the lattice structures between the hexagonal and the monoclinic  $\text{Ga}_2\text{S}_3$  [4]. The significant difference between them appears in the change of the value of the relative intensity of the diffraction peaks as observed for  $\text{Ga}_2\text{S}_3$  deposited onto GaAs substrates [4]. Since this type of crystallization is dominated by high vacancy disorder and because  $\text{Ga}_2\text{S}_3$  is a naturally defective semiconductor with one-third of cation sites being vacant (Ga vacancies) [4], it easily forms an interfacial disorder of metal atoms in some specific interfaces as observed in our structural and morphological analysis.

The data which are presented in Fig. 2 (a) show the capacitance ( $C$ ) –voltage ( $V$ ) characteristics for the Au/ $\text{Ga}_2\text{S}_3$ /Yb device being recorded by an impedance analyzer at signal frequencies of 50-150 MHz, respectively. Generally, literature data on varactors concern information about the  $C - V$  characteristics in the low frequency regions (up to 5.0 MHz). The response of the device at this high frequency range may be regarded as an attractive add in this field. As the figure shows, for all the curves, the device is in the inversion mode till the reverse voltage reaches a specific value that depends on the signal frequency. Above which, the device runs in the depletion mode followed by the accumulation mode during forward biasing. As for example, at 50 MHz, the inversion, depletion and accumulation regions dominate in the applied voltage range of -10.0 – -0.50 V, -0.48-1.38 V and 1.40-10.0 V, respectively. At 120 MHz, the respective voltage ranges are -10.0-0.10 V, 0.12-1.70 V and 1.72-10.0 V. The features of the Au/ $\text{Ga}_2\text{S}_3$ /Yb device at these high frequency values make it suitable for fabrication of voltage controlled field effect transistors with wide voltage tunability which is a feature of varactor devices.

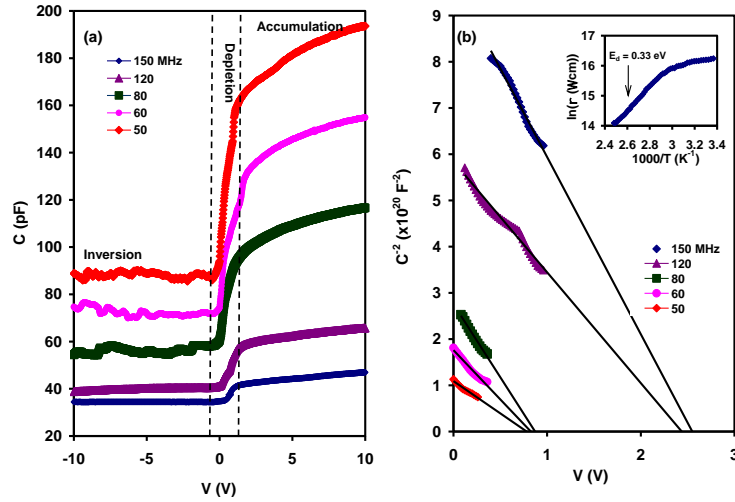


Fig. 2 (a) The capacitance-voltage characteristics and (b) the  $C^{-2} - V$  dependence for the Au/Ga<sub>2</sub>S<sub>3</sub>/Yb diodes.

Physically, at a particular frequency, the behavior of the  $C - V$  characteristics which is observed in Fig. 2 (a) can be explained as follows; for the  $n$ -type Ga<sub>2</sub>S<sub>3</sub> increasing the values of the positive voltage, causes band bending downward. This makes the edge of the conduction band ( $E_c$ ) closer to the Fermi level ( $E_F$ ) at the surface and an accumulation of electrons is obtained at the surface. On the other hand, negative values of applied voltages indicate an upward bending of the bands which increase the distance from the  $E_F$  to the bottom of the  $E_c$  that in turn leads to a depletion of electrons at the surface of  $n$ -type Ga<sub>2</sub>S<sub>3</sub> film. Increasing the surface band bending to a value greater than the built in voltage of the Schottky device ( $V_{bi}$ ) brings the intrinsic level at the surface above the Fermi level and the density of minority carriers (holes) become larger than intrinsic carrier density in the region just below the surface. As the applied reverse voltage reaches a value of  $\sim 2V_{bi}$ , the density of holes increases and at the top of the surface, the type of mobile carriers is inverted with respect to the bulk [8, 9].

In the depletion region, the capacitance voltage characteristic curves are analyzed in accordance with the equation,  $C^{-2} = 2 \left( V_{bi} - V - \frac{kT}{q} \right) / (q\epsilon_s A^2 N_d)$  [8]. The plots of the  $C^{-2} - V$  dependence which are shown in Fig. 2 (b), reveal straight lines with slopes and intercepts that in turn allow determining the density of uncompensated donors ( $N_d$ ) and the built in voltage as well. The semiconductor (Ga<sub>2</sub>S<sub>3</sub>) dielectric constant ( $\epsilon_s$ ) and diode area are substituted as 7.5 [3] and  $3.14 \times 10^{-3} \text{ cm}^2$ , respectively. The resulting physical parameters of the Au/Ga<sub>2</sub>S<sub>3</sub>/Yb device are shown in Fig. 3 (a) and its inset. As the figure reads, increasing the signal frequency increases the built in voltage and decreases the density of uncompensated electrons (inset of Fig. 3 (a)). While, the sensitivity of the built in voltage to the signal frequency is more pronounced above 90 MHz, the decrease in  $N_d$  values are significant below 70 MHz. The decrease in the uncompensated carrier density with increasing frequency can be assigned to the surface charge polarization with the oscillating field. The surface charge polarization decrease the amount of electrons that are available for conduction. This action bends the conduction band down leading to a larger built in voltage [8-10].

In order to investigate the energy band diagram of the Au/Ga<sub>2</sub>S<sub>3</sub>/Yb varactor device, there is a need to determine the work function for the Ga<sub>2</sub>S<sub>3</sub> film. The donors energy level ( $E_d$ ) is determined from the temperature dependent electrical resistivity ( $\rho$ ) measurement which is illustrated in the inset of Fig. 2 (b). The plot of  $\ln(\rho) - T^{-1}$  reveal an activation energy of 0.32 eV. The value indicate that the Fermi level ( $E_F$ ) for the  $n$ -Ga<sub>2</sub>S<sub>3</sub> should be located at 0.16 eV below the conduction band. Since the electron affinity ( $q\chi$ ) in Ga<sub>2</sub>S<sub>3</sub> is 3.30 eV [11], the work function of Ga<sub>2</sub>S<sub>3</sub> is  $q\phi_{Ga_2S_3} = 3.46 \text{ eV}$ . In addition, because the Au and Yb metals work

functions ( $q\phi_m$ ) are 5.34 and 2.51 eV [12], then, the Au and Yb contact metals represent a Schottky ( $q\phi_{Au} > q\phi_{Ga_2S_3}$ ) and Ohmic natures of contact, respectively. Thus, the theoretical Schottky barrier height to the electrons motion for this device is ( $q\phi_b = q\phi_{Au} - q\chi$ ) 2.04 eV. The built in voltage ( $qV_{bi} = q\phi_{Au} - q\phi_{Ga_2S_3}$ ) is 1.88 eV. The energy band diagram for this device is presented in Fig. 3 (b). The value of the built in voltage coincides with the experimentally determined one (Fig. 3 (a)) at 120 MHz. The deviation of the  $qV_{bi}$  from this value at lower frequencies is ascribed to the degree of polarization (inability of charge carriers to follow up with the field direction).

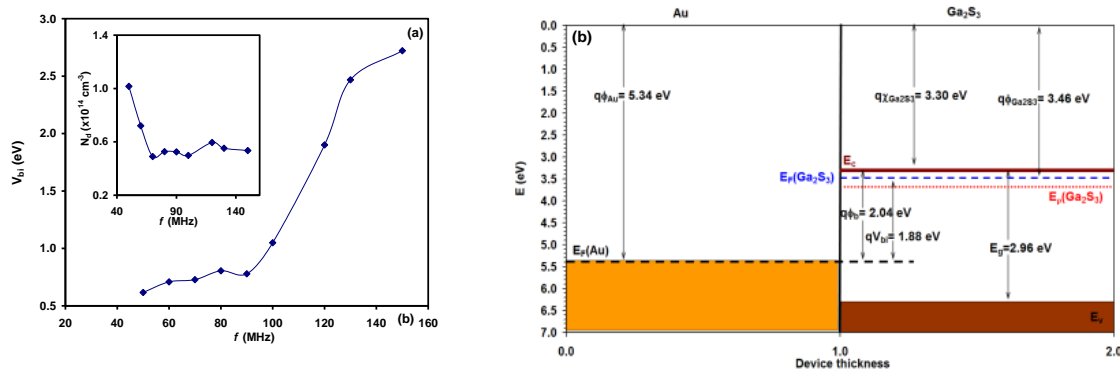


Fig. 3 (a) The frequency dependence of the built in voltage and (b) the energy band diagram for the Au/Ga<sub>2</sub>S<sub>3</sub>/Yb diodes. The inset of (a) display the frequency dependence of the density of uncompensated carriers.

Fig. 4 (a) and (b) display the capacitance spectra for the unbiased and dc biased Au/Ga<sub>2</sub>S<sub>3</sub>/Yb Schottky device. The spectra is recorded in the frequency range of 10-1800 MHz. When small ac signal of Bluetooth energy (0.22 V; 0.0 dBm) is imposed between the device terminals, no signal amplification is observed until a frequency of 850 MHz is reached. In the range of 820-1000 MHz resonance peak followed by antiresonance peaks are observed at 883 and 910 MHz, respectively. The same respective phenomena appears at 1216 and 1242 MHz and at 1264 and 1306 MHz. The signal is amplified 4-6 times in the first two ranges. The resonance-antiresonance first two peaks widths are 27 and 26 MHz. It is also worth noting that the capacitance values at antiresonance positions are negative. On the other hand, when the device is run in the inversion mode ( $V=2.0$  V (19.0 dBm);  $V > V_{bi}$ ) a large signal amplification that reaches two orders of magnitude is observed at 856 MHz. The antiresonance phenomena appeared at 866 MHz and the full wave half maximum for this peak is found to be 10 MHz. The other minor peak (inset of Fig. 4 (b)) showed antiresonance followed by resonance at 1243 and 1254 MHz, respectively. Consistently, the absolute value of the total reactance ( $|X|$ ) is shown in Fig. 4 (c). The reactance exhibit maximum value of 40  $\Omega$  at ~80 MHz for the unbiased device and the maxima of the reactance shifts to ~213 MHz with value of 13  $\Omega$  when it work in the inversion mode. The total reactance exhibit two zero values at 860 and 1249 MHz. These two critical frequencies are of high importance as they define the point of charge storage and parasitic cancelation of capacitance in circuits. On the other hand, the impedance ( $Z$ ) spectra which is displayed in Fig. 4 (d), decreases with increasing signal frequency down to 670 MHz. For higher applied frequencies it re-increases with increasing signal frequency. The impedance never reaches the zero value due to the resistive part of the impedance.

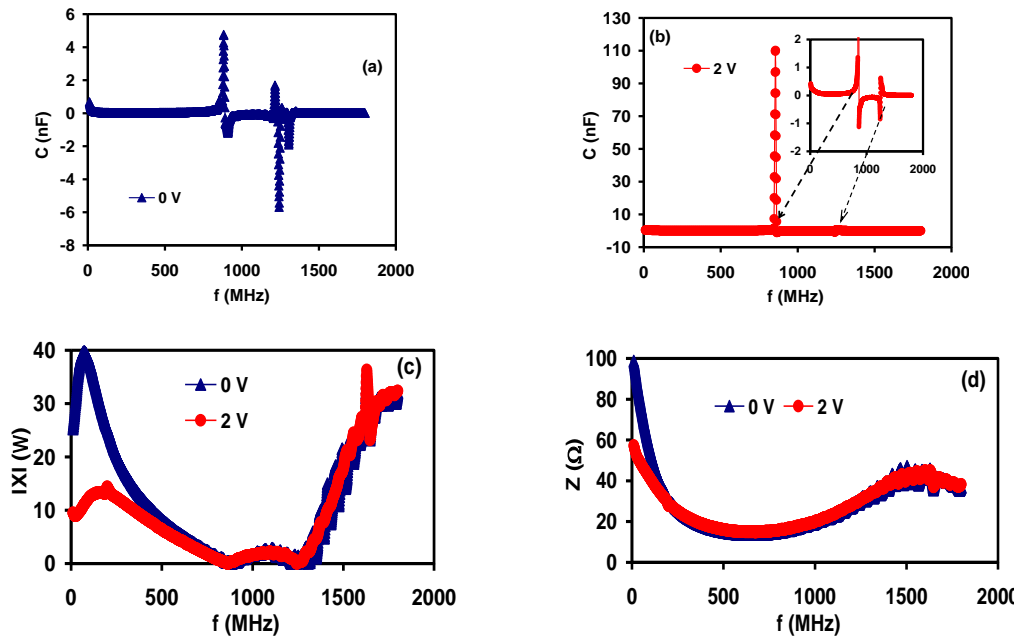


Fig. 4 (a) The unbiased capacitance, (b) the reverse biased capacitance, (c) the reactance and (d) the impedance spectra for Au/Ga<sub>2</sub>S<sub>3</sub>/Yb diodes.

The appearance of these limiting frequencies in the reactance and capacitance spectra may be assigned to the electron-Plasmon interaction at the Au, Yb and Ga<sub>2</sub>S<sub>3</sub> interfaces. Our previous analysis on the dielectric spectra of the Ga<sub>2</sub>S<sub>3</sub> have shown the existence of Plasmon frequencies of 760, 940 and 2260 MHz [3]. The Plasmon frequency is the limit frequency where all signals of frequencies less than it are reflected back and all signals of frequencies higher than it are passed. Those of close value exhibit resonance in the dielectric or capacitance spectra. The shift in the resonance frequency detected here at 860 and 1247 MHz with respect to those observed from light interactions as 760 and 940 MHz can be attributed to the metal sandwich interfacing of the Ga<sub>2</sub>S<sub>3</sub> films. The metals bring an additional constraints to the plasmonic oscillations in the material.

To test the radio and microwave propagation ability in the Au/Ga<sub>2</sub>S<sub>3</sub>/Yb varactor device, the reflection coefficient of the incident ac signal is determined. The reflection coefficient,  $\Gamma = \gamma \angle \theta = (Z_L - Z_0) / (Z_L + Z_0)$ , represents the quality of the impedance match between the source ( $Z_0$ ) and the Au/Ga<sub>2</sub>S<sub>3</sub>/Yb varactor device ( $Z_L$ ). It is a complex quantity, with magnitude  $\gamma$  and polar angle  $\theta$ . The magnitude of the reflection coefficient for the unbiased and reverse biased device is shown in Fig. 5 (a). As seen, it exhibit values of 0.20 near 10 MHz and start increasing with increasing frequency up to ~500 and 600 MHz, respectively. In the region of 500-1400 MHz, the reflection coefficients continuously decrease with increasing frequency and appears to be biasing independent. Above 1500 MHz, it again sharply increases. In general, the  $\gamma$  values are small indicating good impedance matches. The reflection coefficient takes values from -1 for shorts, stays negative for loads  $< Z_0$ , is zero for perfect matches, is positive for loads  $> Z_0$ , and reaches +1 for open loads. The magnitude of the reflection coefficient which is illustrated in Fig. 5 (a) exhibit maximum value of 0.60 at 500 MHz. The  $\gamma$  value sharply falls from 0.60 at 500 MHz to 0.15 at 1400 MHz. It indicates that Au/Ga<sub>2</sub>S<sub>3</sub>/Yb varactor device behave as low pass/ high pass filter device or as band stop device that can be employed in the microwave signal processing technology.

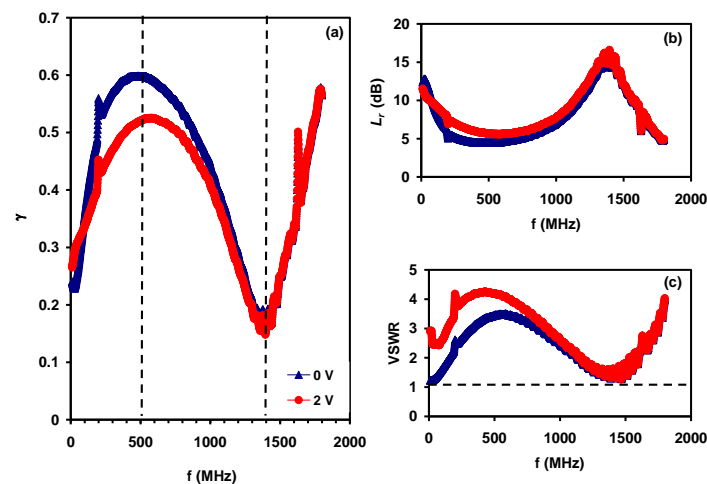


Fig.5 (a) The magnitude of the reflection coefficient, (b) the return loss and (c) the voltage standing wave ratio for Au/Ga<sub>2</sub>S<sub>3</sub>/Yb diodes

The ability of the varactor device to be used as filter is also tested by calculating the absolute value of the return loss ( $L_r = 20\log(\frac{1}{\gamma})$ ) and the voltage standing wave ration ( $VSWR = (1 + \gamma)/(1 - \gamma)$ ) which are displayed in Fig. 5 (b) and (c), respectively. The higher the absolute value of the  $L_r$ , the better the match. It is a measure of the power that is not absorbed by the load and is therefore returned to the source. Thus, the large absolute values of the  $L_r \geq 20$  dB imply a good match. The maximum obtained value for our device is  $\sim 16.7$  dB at 1400 MHz. The value slightly deviate from ideality of band pass/reject filters. For this case the calculation of the VSWR is useful to estimate the peak voltage that can be found on a line under non-ideal match conditions. The VSWR represent common measure of the “goodness” of a match. A perfect match is characterized by a VSWR of 1.0 [13-15], while a short or open circuit produces a VSWR of infinity. For our case which is displayed in Fig. 5 (c), the VSWR value reaches 1.3 at 1400 MHz, which is near perfect impedance match. The significance of this value becomes more clearer if we recall that the VSWR of value of 1.3 corresponds to a power efficiency of  $\sim 98.3\%$ , while VSWR=3.0 corresponds to power efficiency of 75%. For our device the range of 1200-1600 MHz seems to be ideal for data transfer as the power efficiency remains near 90% [14, 15]. The Au/Ga<sub>2</sub>S<sub>3</sub>/Yb device performance is efficient as compared to the broadband RF energy harvesting system designed for harvesting energy from 800 MHz to 2.5 GHz [16]. In that system, a passive voltage amplification schemes and inherent matching technique using higher antenna impedance were used to improve the output voltage of the rectifier. The measured VSWR for that system is  $\sim 2.0$  from 825 MHz to 1.27 GHz and 1.67 GHz to 2.17 GHz [16].

#### 4. Conclusions

In the current work, we have discussed the physical design and properties of the Ga<sub>2</sub>S<sub>3</sub> based Schottky device. The device which represents a metal-semiconductor contacts made of Au and the Ga<sub>2</sub>S<sub>3</sub> is observed to have smart features presented by its variable capacitance properties. A very wide tuning range is detected upon frequency attenuations. In addition, the calculated microwave application parameters presented by the reflection coefficient, the return loss and the voltage standing wave ratio in addition to the negative capacitance effects nominate the device as a band pass/stop filter capable of resonating microwave signals near 1.0 GHz. Such properties of the device make it attractive as a connector between transition lines in telecommunication technology.

## Acknowledgments

This article was funded by the Deanship of Scientific Research (DSR) at King Abdulaziz University, Jeddah. The authors, therefore, acknowledge with thanks DSR for technical and financial support.

## References

- [1] K. Konstantin, L. Ivan, S. Valery, G. Perizat, B. Askar, A. Yuri, *Key Engineering Materials*, **683**(3), 71 (2016).
- [2] Z. Huang, J-G. Huang, K. A. Kokh, V. A. Svetlichnyi, A. V. Shabalina, Yu M. Andreev, G. V. Lanskii, *40th International Conference on Infrared, Millimeter, and Terahertz waves (IRMMW-THz)*, IEEE, Chinese Univ Hong Kong, Hong Kong, PEOPLES R CHINA, pp. 1-2, August 2015.
- [3] S. R. Alharbi, and A. F. Qasrawi, *Plasmonics* (2016). DOI: 10.1007/s11468-016-0357-4
- [4] H. F. Liu, K.K A. Antwi, N. L. Yakovlev, H. R. Tan, L. T. Ong, S. J. Chua, D. Z. Chi, *ACS applied materials & interfaces* **6**(5), 3501 (2014).
- [5] K. F. Abd. El-Rahman, *The European Physical Journal Applied Physics* **37**(2), 143 (2007).
- [6] C. A. Lucas, F. Maroun, N. Sisson, P. Thompson, Y. Grunder, R. Cortès, Ph. Allongue, *The Journal of Physical Chemistry C* **120**(6), 3360 (2016).
- [7] O. Madelung, *Semiconductors: data handbook*. (Springer Science & Business Media, New York, USA, 2012).
- [8] W. Mönch, *Semiconductor surfaces and interfaces*, Springer, New York, USA, 2013.
- [9] K. V. Reich, M. Schechter, and B. I. Shklovskii, *Physical Review B* **91**(11), 115303 (2015).
- [10] A. F. Qasrawi, *Physica Scripta* **89**(6), 065802 (2014).
- [11] N. Seeburrun, E. F. Archibong and P. Ramasami, *Chemical Physics Letters* **467**(1), 23 (2008).
- [12] H. L. Skriver, N. M. Rosengaard, *Physical Review B* **46**(11), 7157 (1992).
- [13] J. F. White, *High frequency techniques: an introduction to RF and microwave engineering*, John Wiley & Sons, New York, USA, 2004.
- [14] Y. Arbaoui, V. Laur, A. Maalouf, P. Quéffélec, D. Passerieux, A. Delias, P. Blondy, *IEEE Transactions on Microwave Theory and Techniques* **64**(1), 271 (2016).
- [15] R. G. M. Oliveira, D. B. Freitas, M. C. Romeu, M. A. S. Silva, A. J. M. Sales, A. C. Ferreira, A. S. B. Sombra, *Microwave and Optical Technology Letters* **58**(5), 1211 (2016).
- [16] M. Arrawatia, M. Sh. Baghini, G. Kumar, In 2016 IEEE MTT-S International Microwave Symposium (IMS), pp. 1-3. IEEE, 345 E 47TH ST, NEW YORK, NY 10017 USA, May 2016.